^{4}He$(p, 2p)^3$H and ^{4}He$(p, pd)^2$H reactions at 156 MeV

R. Frascaria, P. G. Roos,* M. Morlet, N. Marty, A. Willis, V. Comparat, and N. Fujiwara†
Institut de Physique Nucléaire, Orsay, France
(Received 17 March 1975)

Quasifree proton-proton and proton-deuteron scattering cross sections on ^{4}He have been measured and compared with theoretical calculations in the distorted wave impulse approximation. Information on the low components for the proton and deuteron momentum distributions in ^{4}He are deduced.

[NUCLEAR REACTIONS ^{4}He$(p, 2p)$ and ^{4}He(p, pd), $E = 156$ MeV; measured $\sigma(E_1, E_2, \theta_1, \theta_2)$; proton and deuteron momentum distributions in ^{4}He deduced.]

I. INTRODUCTION

Measurements of quasifree knockout reactions on ^{4}He provide information on the ^{4}He ground state wave function and/or the mechanism by which the reaction proceeds. The single particle structure of ^{4}He has been previously investigated by means of the ^{4}He$(p, 2p)^3$H reaction at proton bombarding energies of 65, 85, and 100 MeV[1], 460 MeV[2] and 590 MeV.[3] The data from 65 to 100 MeV show strong energy dependence, and the calculations are rather sensitive to the two body off energy shell effects. On the other hand, the two high energy data points, where off-shell effects are of little importance, appear to be inconsistent. Previous distorted wave impulse approximation (DWIA) calculations by Roos[4] lead to reasonable agreement with the 590 MeV data, but fail to fit the lower energy data. In an attempt to understand the discrepancies and to extract more detailed nuclear structure information, we have measured the ^{4}He$(p, 2p)$-^{3}H reaction at a proton bombarding energy of 156 MeV. This energy is intermediate to the previous results and allows us not only to follow the energy dependence seen at lower energies, but also to reach an energy where off-shell effects are small[5] (~10%). The ^{4}He$(p, 2p)^3$H measurements were made under kinematical conditions which emphasize the low momentum components for protons bound in ^{4}He, and are presented in Sec. II. These data, along with the data at other energies are compared to DWIA calculations in Sec. IV.

In addition the ^{4}He$(p, pd)^2$H reaction has been measured in order to investigate the two deuteron structure of ^{4}He. Again the kinematical conditions were chosen to emphasize the low momentum components. The experimental results are presented in Sec. II, and compared simply to plane wave impulse approximation (PWIA) calculations in Sec. 5.

II. EXPERIMENT

The experiment was performed with the 156 MeV proton beam from the Orsay synchrocyclotron. The beam current was limited to 1 to 2 nA to keep the accidental coincidence rate low and was monitored with an ionization chamber. The beam was focused on a target placed in the center of a 1 m diam scattering chamber. Three identical cylindrical (diameter equal to 18 mm) cryogenic targets with 5 μm Havar windows were mounted on the target ladder. One target was filled with liquid ^{4}He, and the other two targets with liquid hydrogen and deuterium for energy and efficiency calibrations.

The outgoing particles were detected in counter telescopes placed outside of the scattering chamber, the particles exiting through a thin (80 μm) Mylar window. Telescope 1 consisted of a 300 μm silicon surface barrier ΔE detector, a thick plastic scintillator E detector which can stop protons up to 100 MeV and a plastic scintillator veto counter used to reject particles passing through the E detector. The veto counter allowed the rejection of elastically scattered protons, thereby significantly reducing background. The solid angle of this telescope was $\Delta\Omega_1 = 2.4\times10^{-4}$ sr. Telescope 2 was of similar construction, except that the ΔE detector consisted of a thin plastic scintillator. This telescope substended a solid angle of $\Delta\Omega_2 = 6.0\times10^{-4}$ sr.

For each telescope a fast coincidence-anticoincidence (~15 ns) was established between the ΔE, E, and veto counters. The fast coincidence (< 3 ns) between the two telescopes was performed using the signals from the two E detectors in conjunction with a time-to-amplitude converter (TAC). The range of the TAC was chosen to allow the simultaneous storage of the real and accidental co-

incidence bursts which are separated by the rf period (48 ns). For each coincidence event four linear signals were amplified, gated by the coincidence requirements, and sent to analog-to-digital converters (ADC). These four signals were: the pulse heights from each of the two E detectors, the pulse height from the Si surface barrier ΔE detector, and the output of the TAC. The ADC outputs were stored on magnetic tape by means of a 2116B Hewlett-Packard computer for subsequent detailed analysis with a larger computer. During the experiment various biparametric displays such as E_1 versus E_2 or ΔE_1 versus E_1 were displayed using the Hewlett-Packard, in order to monitor the experiment.

The energy calibration and efficiency as a function of energy for each telescope were obtained by measuring p-p and p-d elastic scattering using the liquid hydrogen and deuterium targets. These results were compared with previously accurately measured cross sections[6,7] to extract the detector efficiency. Such a procedure removes many systematic errors, and avoids the necessity of correcting the data for losses due to nuclear reactions in the scintillators and multiple scattering. The overall absolute error, apart from the normal statistical error, was estimated to be 5% for the

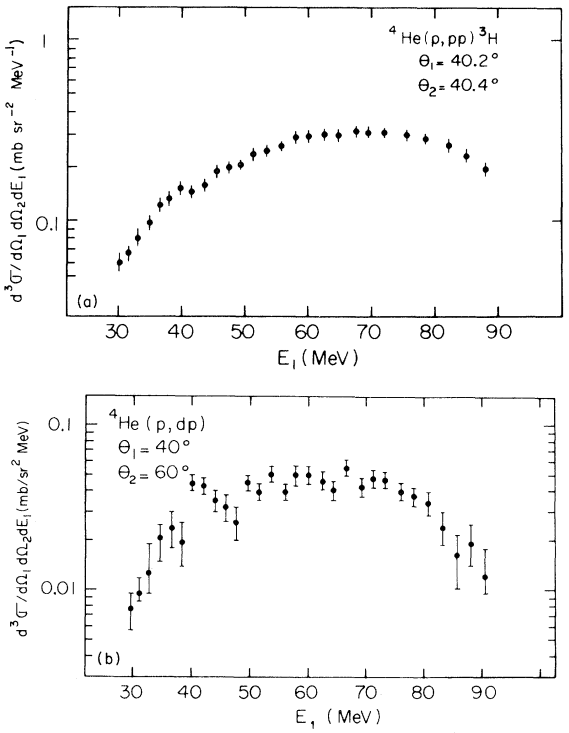

FIG. 1. The three-body cross sections at quasifree angle pairs: (a) the ^{4}He(p, $2p$)^{3}H reaction, and (b) the ^{4}He(p, pd)d reaction.

^{4}He(p, $2p$)^{3}H reaction and 7% for the ^{4}He(p, pd)^{2}H reaction.

In replaying the experimental data, particle identification was performed for telescope 1, accidental coincidence events subtracted, and the real coincidence events corresponding to the three-body kinematic locus for the particular reaction projected onto the proton energy axis. Contributions to the resultant energy sharing spectra from interfering reactions, which arise due to the lack of particle identification on telescope 2, were found to be negligible either due to the separation of the various kinematic lines or due to their small yield. The energy resolution in the binding energy spectra was typically 2.8 MeV thereby removing any significant four-body contributions to the energy sharing spectra. In general, the region of four-body breakup was weakly populated compared to the three-body breakup.

The three-body cross sections for the two reactions at quasifree angle pairs (angle pairs for which zero recoil momentum of the undetected particle is kinematically allowed) are presented in Figs. 1(a) and 1(b). Both spectra show a pronounced broad peak characteristic of S-state quasifree knockout. The ^{4}He(p, pd)^{2}H cross section is approximately a factor of 6 smaller than the ^{4}He(p, $2p$)^{3}H one reflecting in large part the differences in the p-p and p-d two-body cross sections.

III. THEORY

Assuming the three-body breakup reaction to be dominated by the knockout process, one generally analyzes the results within the framework of the PWIA or DWIA. In these approximations one assumes that the three-body cross section for the $A(a, ab)B$ reaction factorizes as[8,9]

$$\frac{d^3\sigma}{d\Omega_a d\Omega_b dE_a} = (\mathrm{PSF})\frac{d\sigma}{d\Omega}\Big)_{a-b} N_b |\varphi(-\vec{p}_B)|^2 , \qquad (1)$$

where PSF is a known kinematic factor, and N_b is a spin-isospin factor which we have taken as $N_p = 2$ for the ^{4}He(p, $2p$)^{3}H reaction and $N_d = 3$ for the ^{4}He(p, pd)^{2}H reaction.

The quantity $d\sigma/d\Omega)_{a-b}$ is a half-off-energy shell two-body cross section for the interaction of particles a and b. For the (p, $2p$) reaction, off-shell cross sections have been calculated[5] and compared to various on-shell prescriptions for the choice of $d\sigma/d\Omega)_{pp}$. At the present energy of 156 MeV and under the kinematic conditions of our experiment, the differences between various on-shell and off-shell cross sections are small (~10%). Thus the use of the Stern-Chamberlain on-shell approximation[10] is sufficiently accurate. At higher energies the differences are even smaller and the method

of choosing $d\sigma/d\Omega)_{pp}$ is of little consequence —at least for low recoil momentum data.

In the case of the (p, pd) reaction no calculations of the two-body off-shell cross sections have been made. We have therefore investigated various possible on-shell prescriptions for the choice of $d\sigma/d\Omega)_{pd}$. The differences between these prescriptions are discussed in Sec. V.

The quantity $|\varphi(-\vec{p}_B)|^2$ represents the momentum distribution (distorted or undistorted) of particle b in the target nucleus. Due to the direct interaction hypothesis, in the PWIA the momentum q of the particle b in ^{4}He is exactly opposite to the recoiling momentum of the core $\vec{q} = -\vec{p}_B$. The distorted momentum distribution in the DWIA is given:

(i) For the ^{4}He$(p, 2p)^3$H reaction by

$$\varphi(-\vec{p}_B) \propto \int d^3\vec{\xi} d^3\vec{r}\, \chi^{(-)*}_{\vec{p}_1}(\vec{r})\chi^{(-)*}_{\vec{p}_2}(\vec{r})\psi_4(\vec{r}, \vec{\xi})\psi_3(\vec{\xi})\chi^{(+)}_0(\gamma\vec{r})e^{i\vec{q}\cdot\vec{r}} \tag{2}$$

with $\xi^2 = \xi_1^2 + \xi_2^2$ [see Fig. 2(a)].

The χ's are the distorted waves for the incoming and outgoing protons relative to the triton core. The value of γ is given by $\gamma = m_B/(m_b + m_B) = \frac{3}{4}$.

The ^{4}He and ^{3}H wave functions, ψ_4 and ψ_3, contain, respectively, three and two space coordinates with respect to which they must be normalized to unity.

(ii) For the ^{4}He$(p, pd)^2$H reaction by

$$\varphi(-\vec{p}_B) \propto \int d^3\vec{\rho}_1 d^3\vec{\rho}_2 d^3\vec{r}'\, \chi^{(-)*}_{\vec{p}_1}(\vec{r}')\chi^{(-)*}_d(\vec{r}')\psi_4(\vec{\rho}_1, \vec{\rho}_2, \vec{r}')\Phi_2(\vec{\rho}_1)\Phi_2(\vec{\rho}_2)\chi^{(+)}_0(\gamma r)e^{i\vec{q}\cdot\vec{r}'} \tag{3}$$

with $\vec{\rho}^2 = \vec{\rho}_1^{\,2} + \vec{\rho}_2^{\,2}$ [see Fig. 2(b)] and where now the χ's are the distorted waves for the incoming proton and outgoing proton and deuteron relative to a deuteron core. Here $\gamma = \frac{1}{2}$. The two deuteron wave functions, $\Phi_2(\vec{\rho}_1)$ and $\Phi_2(\vec{\rho}_2)$, are normalized to unity.

In both cases, if an independent particle model is assumed to describe either an S-state proton in ^{4}He as

$$\psi_4(\vec{r}, \vec{\xi}) = \Phi_3(\vec{\xi}) \cdot u_p(\vec{r})$$

or a S-state deuteron as

$$\psi_4(\vec{\rho}_1, \vec{\rho}_2, \vec{r}') = \Phi_2(\vec{\rho}_1) \cdot \Phi_2(\vec{\rho}_2) \cdot u_d(\vec{r}')\,.$$

Equations (2) or (3) reduce to

$$\varphi(-\vec{p}_B) \propto \int d^3\vec{r}\, \chi^{(-)*}_a(\vec{r})\chi^{(-)*}_b(\vec{r})\, u_b(\vec{r})\chi^{+}_0(\gamma r)e^{i\vec{q}\cdot\vec{r}} \tag{4}$$

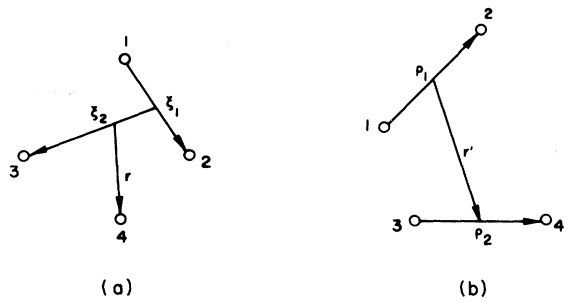

FIG. 2. Space coordinate definitions for the breakup of ^{4}He: (a) $p + {}^3$H, and (b) two deuterons.

with

$$\int |u_b(\vec{r})|^2 d^3\vec{r} = 1\,.$$

In the plane wave limit (PWIA) the χ's become plane waves and $\varphi(-\vec{p}_B)$ is then the Fourier transform of $u_b(\vec{r})$.

IV. ^{4}He$(p,2p)^3$H REACTION

A. Experimental momentum distribution

For simplicity in comparing the present results with other experimental data, we have generated the experimental distorted momentum distribution, i.e.,

$$\varphi_{\rm exp}{}^2(p_3) = \frac{d^3\sigma_{\rm exp}}{d\Omega_1 d\Omega_2 dE_1} \Big/ \left[(\mathrm{PSF})\frac{d\sigma}{d\Omega}\right)_{pp} N_p\Big],$$

where p_3 is the triton recoil momentum. The resultant distribution is plotted versus p_3 on Fig. 3 along with the same distributions from the 100 MeV [1] and 590 MeV [3] data.

One observes firstly that the present energy sharing data (156 MeV) for the quasifree angle does not define the distribution to very large values of recoil momentum. In terms of the PWIA this implies that the experiment does not explicitly measure the high momentum components ($p_3 > 140$ MeV/c) of the proton in ^{4}He except as they are reflected in the normalization. The full width at half-maximum (FWHM) of this distribution is 210 ± 12 MeV/c. Secondly, the ^{4}He$(p, 2p)^3$H data

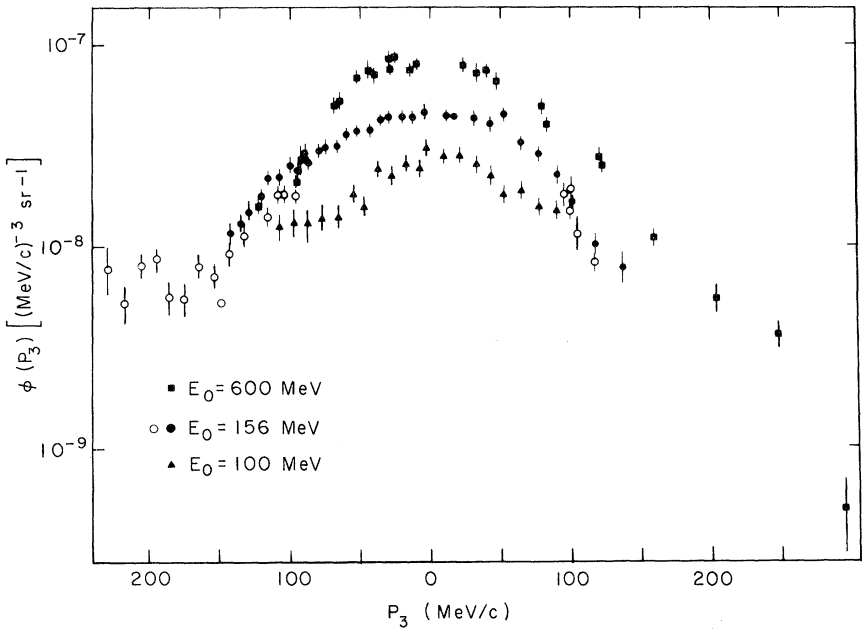

FIG. 3. The experimental distorted momentum distributions of a proton in ^{4}He at 100 MeV (▲), 156 MeV (○, ●), and 600 MeV (■) incident proton energy versus the triton recoil momentum.

taken at the angles ($\theta_1 = 60°$, $\theta_2 = -40°$), which contains higher momentum components, agree reasonably well with the quasifree angle data for $p_3 < 140$ MeV/c, but is rather flat for p_3 ranging from 150 to 255 MeV/c.

In comparison with the other experimental data our values appear to be at least reasonably consistent. The 100 MeV energy sharing data does not define a significant portion of the distribution, and so one can only say that the magnitude of φ^2 is smaller, as would be expected from the increased importance of distortion effects at these lower energies. The 590 MeV data was obtained from a coplanar symmetric angular distribution, and therefore measures the distribution to much larger momenta. However, the distribution is not symmetric about $p_3 = 0$. In comparing these data to the present data, we can only comment that the shape of the right hand side of the 590 MeV distribution agrees reasonably well with our results. In addition the φ^2 shows a further reduction in distortion effects as the energy increases.

B. DWIA calculations

We start with Eq. (4) using a single particle wave function $u_p(r)$ of the Eckart form given by Lim.[11] The DWIA calculations have been carried out at 156 MeV using the code of Chant[12] in the same frame as previous calculations performed by Roos.[4] The calculated momentum distribution, with plane waves as well as distorted waves, are compared to the experimental data in Fig. 4. One observes that the effect of the distortion is to reduce $|\varphi(0)|^2$ by almost a factor of 2 and to slightly broaden the distribution. However, the calculated $|\varphi(0)|^2$ is still about a factor of 2 larger than the experimental data.

We compared these results with DWIA calculations using the same wave function $u_p(r)$ but where the χ's are obtained by integrating the optical potentials along the classical path of the interacting particles (WKB method). Similar shapes are obtained (Fig. 4) although the WKB calculation is somewhat narrower and shows slightly more attenuation. Unfortunately, no specific conclusions

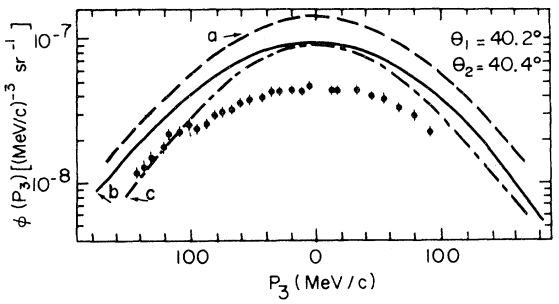

FIG. 4. PWIA (curve a), DWIA of Ref. 4 (curve b), DWIA with distortion obtained with a WKB method (curve c) calculations compared with the experimental distorted momentum at $E_0 = 156$ MeV versus the triton recoil momentum.

concerning the two methods can be reached, since the optical potentials in the two sets of calculations were different due to limitations in the codes.

In order to investigate the discrepancy in magnitude in more detail, we have compared the magnitudes of the experimental momentum distributions for zero recoil momentum $[\varphi^2(0)]$ plotted as a function of energy to the DWIA calculations of Ref. 4. These results are presented in Fig. 5 where the 460 MeV data are included. This figure strongly suggests a discrepancy between the two high energy points. We see that the calculation agrees only with the 590 MeV data, whereas, if we renormalize the calculation by 0.5, it agrees with the other five data points.

Thus we can only conclude that if the 590 MeV data point is correct, then the DWIA treatment presented here and in Ref. 4 is incorrect either due to an improper choice of optical potentials or due to a failure of the DWIA to describe the reaction mechanism. With respect to the first point we comment only that for energies greater than 156 MeV *reasonable* variations in the distorting potentials produce less than about a 20% change in magnitude. With respect to the failure of the DWIA it is worthwhile mentioning that the 156 MeV data for the second pair of angles (60°, −40°) (see Sec. IV A) showed possible contributions from higher order processes, at least for about 15% of the maximum in φ^2.

On the other hand if one assumes that the 460 MeV data are correct, then the DWIA calculation gives the right trend as a function of energy and one must question the appropriateness of the Lim wave function in describing a bound proton in ^4He. In this respect we have investigated several other possible wave functions which are presented in the next subsection.

C. ^4He wave function

In order to investigate the effects of various ^4He wave functions on the theoretical $^4He(p, 2p)^3H$ cross section, we have calculated the distorted momentum distribution $|\varphi(p_3)|^2$ at 156 MeV for three wave functions; the resultant momentum distributions are presented in Fig. 6.

(a) An independent particle model is assumed to describe an S state proton in ^4He. The Eckart form given by Lim is used in which the parameters have been chosen to fit electron scattering (see Fig. 7, curve a). The distorted momentum distribution is calculated by Eq. (3) with the WKB method. As indicated in the previous section, the magnitude is too large by a factor of 2 compared to the experimental points (Fig. 6, curve a).

Due to the important difference between the binding energy of the triton and the ^4He, it seems to be more reasonable to describe separately the ^4He target and the triton core. The distorted momentum is then calculated by means of Eq. (2). Two different trials have been performed.

(b) The ^4He and ^3H nuclei are both described by oscillator wave functions, the root mean square radii being, respectively, $\langle R_4\rangle = 1.6$ fm and $\langle R_3\rangle = 1.7$ fm. The fit to the ^4He charge form factor is shown in Fig. 7, curve b. At large momentum transfers the oscillator wave function obviously does not reproduce the minimum. The resultant momentum distribution is similar to independent particle model (a). Therefore, as suggested in Ref. 14, the ^4He rms radius has been slightly changed from 1.6 to 1.5. The charge form factor is still fitted at low transfers (see Fig. 7, curve c) but the high transfer region is enhanced. The distorted momentum distribution shown in Fig. 6, curve b is significantly broader and consequently

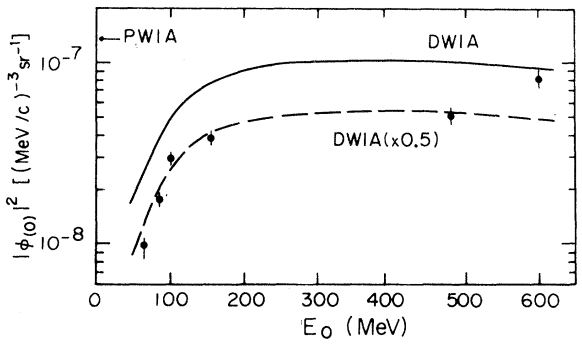

FIG. 5. Experimental momentum distributions of a proton in ^4He for zero recoil momentum plotted as a function of energy and compared to the DWIA calculations of Ref. 4.

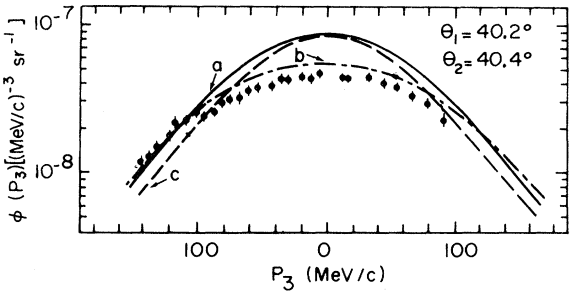

FIG. 6. Comparison between various ^4He wave functions in DWIA calculations for the $^4He(p, 2p)^3H$ reaction. The wave functions used are (a) a single particle wave function of Ref. 11, (b) oscillator wave functions for ^3H ($\langle R_3\rangle = 1.7$ fm) and ^4He ($\langle R_4\rangle = 1.5$ fm), (c) Fabre de la Ripelle and co-workers (Ref. 15) ^3H and ^4He wave functions.

$|\varphi(0)|^2$ is lower, which produces reasonable agreement with the $(p, 2p)$ data.

(c) Triton and ^{4}He wave functions from theoretical calculations by Fabre de la Ripelle and coworkers[15] have then been used. These wave functions are extracted from the resolution of the three- and four-body bound states in the hyperspherical expansion method. The potential used for the triton is a high repulsive soft core central potential whose parameters are determined by fitting the ^{3}H binding energy as well as the ^{3}He and ^{3}H charge form factors. The use of the same nucleon-nucleon potential was not possible for the four-body case and Ballot used a nonrealistic Volkov potential fitting only the ^{4}He binding energy. The distorted momentum distribution calculated with these functions is shown in Fig. 6, curve c. Compared to the calculation of Sec. IV C a, the distribution is narrower and the magnitude only slightly smaller.

Thus, the various wave functions obviously have a large effect on the calculated momentum distribution. It is possible to obtain reasonable agreement with the data (Sec. IV C b) but it is rather difficult to reach any conclusions before comparing with calculations using a more realistic ^{4}He wave function.

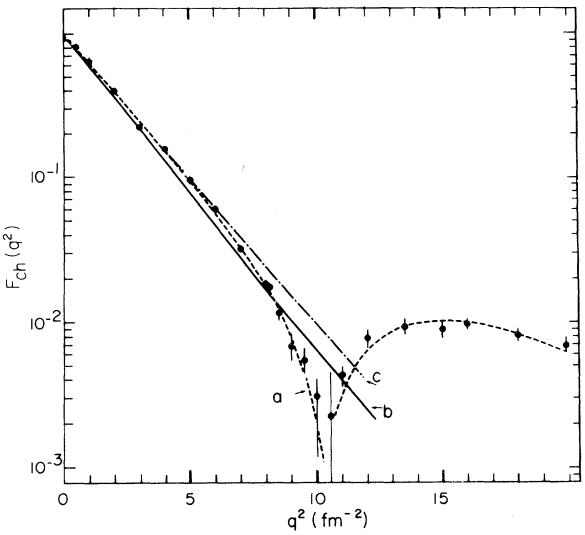

FIG. 7. Experimental ^{4}He charge form factor (Ref. 16) compared with the theoretical one using a single particle wave function with correlations Ref. 11 (curve a), or an oscillator wave function with $\langle R_4\rangle = 1.6$ (curve b) or $\langle R_4\rangle = 1.5$ (curve c).

V. ^{4}He$(p,pd)^2$H REACTION

A. Experimental momentum distribution

The experimental distorted momentum is now extracted from

$$|\varphi_{\rm exp}(p_3)|^2 = \frac{d^3\sigma_{\rm exp}}{d\Omega_1 d\Omega_2 dE_1} \Big/ \left[(\mathrm{PSF})\frac{d\sigma}{d\Omega}\right)_{pd} N_d\Big],$$

where p_3 is the deuteron recoil momentum, $d\sigma/d\Omega)_{pd}$ is a free p-d cross section taken for various kinematical approximations which conserve the momentum transfer between the detected deuteron and the incident proton. The first approximation (Ap. I) conserves the transfer momentum and the center of mass energy in the ingoing channel. Then the free p-d cross section must be taken at the laboratory energy,

$$E_{\rm in} = E_0 + \tfrac{1}{2}E_3 + [E_0 E_3/2]^{1/2}\cos\theta_3$$

and at the laboratory deuteron angle,

$$\theta_{\rm in} = \arcsin\left\{\frac{1}{2}\frac{2 - 9[E_2 + E_0 - 2(E_0E_3)^{1/2}\cos\theta_2]}{8E_{\rm in}}\right\}^{1/2},$$

where E_0, E_3, and θ_3 are, respectively, the lab incident proton energy, the energy, and angle of the recoiling deuteron.

The second approximation (Ap. II) is rather similar to Ap. I, but in the formulas $E_{\rm in}$ is replaced by $E'_{\rm in} = E_{\rm in} - \frac{3}{2}E_s$ where E_s is the energy separation of a deuteron in ^{4}He. In the third one (Ap. III) the momentum transfer is conserved as well as the center of mass energy in the outgoing channel. Then the free p-d cross section is taken at an energy

$$E_{\rm out} = \tfrac{1}{2}E_1 + E_2 - (E_1E_2/2)^{1/2}\cos(\theta_2 - \theta_1)$$

and a deuteron angle

$$\theta_{\rm out} = \arcsin\left\{\frac{1}{2}\frac{2 - 9[E_2 + E_0 - 2(E_0E_2)^{1/2}\cos\theta_2]}{8E_{\rm out}}\right\}^{1/2},$$

where E_1, θ_1, E_2, and θ_2 are, respectively, the lab energy and angle of particle 1 (deuteron) and particle 2 (proton) in the outgoing channel.

The $d\sigma/d\Omega)_{pd}$ as a function of E and θ were obtained from a linear interpolation between the experimental free p-d cross sections measured at 95 MeV [10] and 156 MeV.[7]

The importance of the off-shell effects in the p-d interaction is not known. The off-shell energy is already important at $p_3 = 0$, since the ratio of the final to the initial momentum of the incident proton relative to the knocked-out deuteron is 0.8 and reaches 0.7 at $p_3 = 1$ fm^{-1}.

The three prescriptions lead to different kinematical conditions for the choice of the free p-d cross section. For a pair of angles of the ^{4}He$(p, pd)d$ reaction the three approximations give very simi-

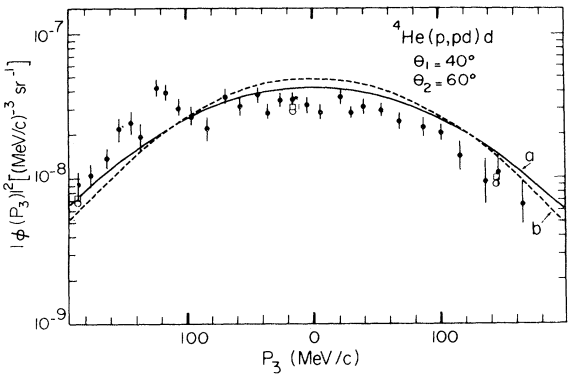

FIG. 8. Experimental distorted momentum distribution of a deuteron in ^{4}He obtained when using Ap. I (○ represents Ap. II and □ Ap. III) and compared to PWIA calculations for $\theta_1 = 40°$, $\theta_2 = 60°$.

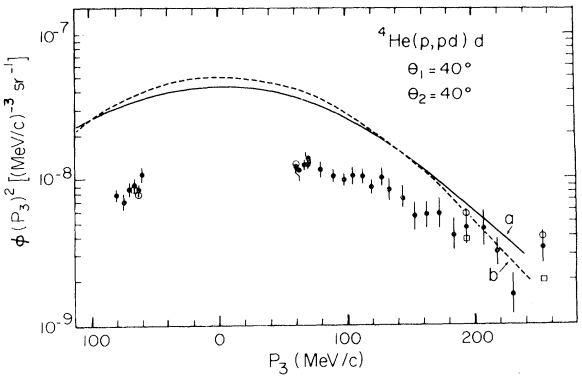

FIG. 9. Experimental distorted momentum distribution obtained using Ap. I (○ represents Ap. II and □ Ap. III) and compared to PWIA calculations for $\theta_1 = 40°$, $\theta_2 = 40°$.

lar results as is shown in Fig. 8 where the $|\varphi(p_3)|_{\text{exp}}^2$ for $\theta_1 = 40°$, $\theta_2 = 60°$ is plotted. The $d\sigma/d\Omega)_{pd}$ values are taken for Ap. I and the various symbols represent $|\varphi(p_3)|_{\text{exp}}^2$ when Ap. II or III are used. The range of variation for $d\sigma/d\Omega)_{pd}$ is then between about 0.3 and 0.5 mb/sr. Due to the strong variations of $d\sigma/d\Omega)_{pd}$ with transfer and energy, changing the kinematical conditions for the ^{4}He$(p, pd)d$ reaction changes the mean value of the free $d\sigma/d\Omega)_{pd}$ cross section. One can see this effect comparing Fig. 8 with Fig. 9. In Fig. 9 are plotted the $|\varphi(p_3)|_{\text{exp}}^2$ for $\theta_1 = 40°$, $\theta_2 = 40°$ where now $d\sigma/d\Omega)_{pd}$ is varying between 0.7 to 1 mb/sr. Again the results are plotted with Ap. I, and the various symbols indicate the values at various momentum transfers given by the other two approximations. As for the $\theta_1 = 40°$, $\theta_2 = 60°$ data, the three different prescriptions lead to similar results, except at high momentum transfer (~260 MeV/c) where the various prescriptions can change the data by a factor of 2.

B. PWIA calculations

In spite of the unknown off-energy-shell effects and the variations with the different kinematical prescriptions, we compare the experimental momentum distribution to PWIA calculations. The overlap between the ^{4}He nucleus and two deuterons is calculated with the ^{4}He oscillator wave function which was used in Sec. IV C b with $\langle R_4 \rangle = 1.5$. The deuterons are described by the usual Hulthen wave function

$$\Phi_2 = N_2[\exp(-a\rho) - \exp(-b\rho)]/\rho$$

with $a = 0.231$ fm^{-1} and $b = 1.438$ fm^{-1}. The calculation by means of Eq. (3) yields the curves labeled a in Figs. 8 and 9. The curve b is the same calculation but with $\langle R_4 \rangle = 1.6$. The experimental shape at the quasifree angle (Fig. 8) is reproduced rather well with a FWHM of about 210 Mev/c. There are obvious difficulties, as evidenced by the fact that the second pair of angles (Fig. 9) is not well fitted and the fact that the PWIA magnitude agrees with the data, although we would expect distortion effects to reduce the calculated ϕ^2. However, until reasonable DWIA calculations can be performed, we can only conclude that the data are consistent with the deuteron knockout interpretation.

VI. CONCLUSIONS

Our ^{4}He$(p, 2p)^3$H results at 156 MeV seem to be consistent with other experimental data at medium energies. The quasifree p-p scattering between 100 and 600 MeV, due to the low distortion effects and the weak dependence on various kinematical prescriptions, seems to allow the determination of a correct momentum distribution for low momenta (~1 fm^{-1}). However, a more realistic description of the ^{4}He wave function is needed.

For the quasifree p-d reaction, the uncertainties coming from the kinematical prescriptions, the unknown off-energy-shell and distortion effects, prevent the extraction of any detailed nuclear information.

*Present address: University of Maryland, College Park, Maryland 20742.
†Present address: University of Kyoto, Kyoto, Japan.

[1]H. G. Pugh *et al.*, Phys. Lett. 46B, 192 (1973).
[2]H. Tyren, S. Kullander, O. Sundberg, R. Ramachandran, P. Isacson, and T. Berggren, Nucl. Phys. 79, 321 (1966).
[3]C. F. Perdrisat *et al.*, Phys. Rev. 187, 1201 (1969).
[4]P. G. Roos, Phys. Rev. C 9, 2437 (1974).
[5]E. F. Redish, G. J. Stephenson, and G. M. Lerner, Phys. Rev. C 2, 1665 (1970).
[6]C. Caversazio and A. Michalowicz, J. Phys. (Paris) 21, 314 (1960).
[7]K. Kuroda, Ph.D. thesis, Orsay, 1966 (unpublished); and K. Kuroda, A. Michalowicz, and M. Poulet, Nucl. Phys. 88, 33 (1966).
[8]G. Jacob and Th. A. J. Maris, Rev. Mod. Phys. 38, 121 (1966); 45, 6 (1973).
[9]T. Berggren and G. Jacob, Nucl. Phys. 47, 481 (1963).
[10]O. Chamberlain and M. O. Stern, Phys. Rev. 24, 666 (1954); R. Frascaria, V. Comparat, N. Marty, M. Morlet, A. Willis, and N. Willis, Nucl. Phys. A178, 307 (1971).
[11]T. K. Lim, Phys. Lett. 44B, 341 (1973).
[12]N. S. Chant and R. Woody, III, Progress Report, Univ. of Maryland, 1973 (unpublished).
[13]R. W. McAllister and R. Hofstadter, Phys. Rev. 102, 851 (1956); R. Hofstadter, Rev. Mod. Phys. 28, 214 (1956).
[14]J. P. Repellin, P. Lehmann, J. Le François, and D. B. Isabelle, Phys. Lett. 16, 179 (1965).
[15]M. Beiner and M. Fabre de la Ripelle, Nuovo Cimento Lett. 1, 584 (1971); J. L. Ballot, M. Beiner, and M. Fabre de la Ripelle, in *Proceedings of the International Symposium on the Present Status and Novel Developments in the Nuclear Many-Body Problem, Rome, Italy, September 19–23, 1972,* edited by F. Calogero and C. Ciofi Degli Atti (Editrice Compositori, Bologna, 1973).
[16]Frosch *et al.*, Phys. Rev. 160, 874 (1967).